Nanoscale Advances

ROYAL SOCIETY OF CHEMISTRY

PAPER

View Article Online
View Journal | View Issue

Cite this: *Nanoscale Adv.*, 2024, **6**, 4230

A tilapia skin-derived gelatin hydrogel combined with the adipose-derived stromal vascular fraction for full-thickness wound healing†

Yanan Luo,‡[ab] Manfei Fu,‡[a] Ziyi Zhou,[c] Xiaopei Zhang,[ad] Qingxia Guo,[ae] Yawen Wang,[ad] Weina Zhang,[b] Yuanfei Wang,*[f] Zhenyu Chen*[b] and Tong Wu *[ad]

Received 22nd April 2024
Accepted 18th June 2024

DOI: 10.1039/d4na00332b

rsc.li/nanoscale-advances

Biomaterials are widely used in regenerative medicine to repair full-thickness skin defect wounds. The adipose-derived stromal vascular fraction (SVF) shows pro-regenerative properties, however, the *ex vivo* biological activity of SVF is suppressed due to the lack of an external scaffold. Tilapia skin, as a sustained and recyclable biomaterial with low immunogenicity, was applied in the preparation of a hydrogel. The mixture of tilapia skin-derived gelatin and methacrylic anhydride as a scaffold facilitated the paracrine function of SVF and exerted a synergistic effect with SVF to promote wound healing. In this study, 30% (w/v) SVF was added to methacrylate-functionalized tilapia skin gelatin and subsequently exposed to UV irradiation to form a three-dimensional nano-scaffolding composite hydrogel (FG-SVF-3). The effects of paracrine growth factors, neovascularization, and collagen production on wound healing were extensively discussed. FG-SVF-3 displayed a pronounced wound healing ability *via in vivo* wound models. The FG-SVF-3 hydrogel enhanced the biocompatibility and the expression of EGF, bFGF, and VEGF. FG-SVF-3, as a promising wound dressing, exhibited superior ability to accelerate wound healing, skin regeneration, and wound closure.

Introduction

The proliferation of fibroblasts and vascular endothelial cells plays a vital role in wound repair for full-thickness skin defects.[1] The adipose-derived stromal vascular fraction (SVF) enriches mesenchymal stem cells and the extravascular matrix and can induce the proliferation and migration of skin fibroblasts and vascular endothelial cells through a paracrine mechanism, consequently exhibiting pro-regenerative properties.[2] However, due to the instability and complexity of subjects, directly transplanted stem cells show poor retention ability.[3] It is unlikely for SVF to maintain high biological activity *ex vivo* without the protection of an external scaffold.[4] Regulating the paracrine function of SVF through external scaffolds to promote tissue regeneration could be an effective approach.[5] Due to the bioactivity and porosity of hydrogels, they are widely employed as biological scaffolds to promote the growth and differentiation of cells.[6] Previous studies described that gelatin possessed cell adhesive properties and matrix metalloproteinase attachment sites. This could significantly reduce the antigenicity associated with thermal denaturation and be widely applied in preparing hydrogels for tissue engineering applications.[7] However, due to zoonotic virus infection and other social issues, the use of mammalian-sourced gelatin is strictly limited.[8] In the present study, gelatin was extracted from tilapia skin[9] and combined with methacrylic anhydride (MA), commonly used in preparing UV cross-linked hydrogels.[10] A novel composite hydrogel was prepared with extracted SVF and tilapia skin-derived gelatin *via* photo-crosslinking to evaluate its ability to accelerate wound healing.

Results and discussion

Fig. 1a–c show the three states from tilapia skin to the gelatin methacryloyl (GelMA) hydrogel. As shown in Fig. 1d, MA was cross-linked with the amino group derived from tilapia skin gelatin under UV irradiation for 30 s to form fish skin GelMA hydrogels. The collection and extraction of SVF were carried out

[a]*Medical Research Center, The Affiliated Hospital of Qingdao University, Qingdao 266000, China. E-mail: twu@qdu.edu.cn*

[b]*Department of Cosmetic and Plastic Surgery, The Affiliated Hospital of Qingdao University, Qingdao 266000, China. E-mail: czy.plastic@126.com*

[c]*Department of Plastic, Reconstructive and Cosmetic Surgery, Xinqiao Hospital, Army Medical University, Chongqing 400037, China*

[d]*Shandong Key Laboratory of Medical and Health Textile Materials, Collaborative Innovation Center for Eco-textiles of Shandong Province and the Ministry of Education, College of Textile & Clothing, Qingdao University, Qingdao 266071, China*

[e]*Institute of Neuroregeneration & Neurorehabilitation, Department of Pathophysiology, School of Basic Medicine, Qingdao University, Qingdao 266071, China*

[f]*Qingdao Stomatological Hospital Affiliated to Qingdao University, Qingdao 266001, China. E-mail: zhizunbao19@163.com*

† Electronic supplementary information (ESI) available. See DOI: https://doi.org/10.1039/d4na00332b

‡ Y. Luo and M. Fu contributed equally to this study.

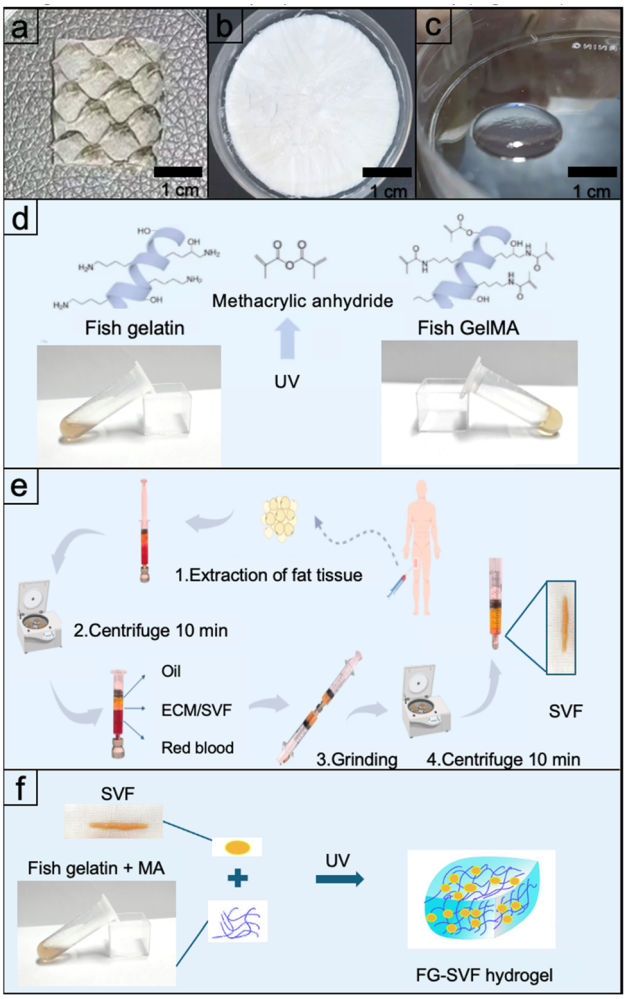

Fig. 1 (a–c) Photographs showing the (a) tilapia fish skin, (b) gelatin, and (c) GelMA hydrogel. (d–f) Schematic illustration of the (d) preparation of fish GelMA, (e) extraction for SVF, and (f) preparation of the composite hydrogels.

according to the procedures previously reported (Fig. 1e).[11] The mixture of gelatin and MA was used as a cell adhesion scaffold, and SVF was subsequently added to the mixture to form a composite solid hydrogel *via* photo-crosslinking. Finally, a three-dimensional nano-scaffolding composite hydrogel with cell growth function was prepared successfully (Fig. 1f).

Since the hydrogels could not be fabricated with SVF content greater than 30% (w/v) in our pre-experiments, a series of composite hydrogels with different SVF ratios (10%, 20%, and 30% (w/v)) were prepared for investigation (Fig. 2a and b). Scanning electron microscopy (SEM) images (Fig. 2c) illustrated the addition of various SVF ratios resulting in larger pore size of hydrogels, compared with the intrinsic porous structure of the hydrogel,[12] which was favorable for gas exchange and nutrient transport, leading to a more pronounced healing-promoting effect of the wound dressings. In addition, as shown in Fig. S1,† the hydrogels had a specific compressive modulus within 0.1–10 kPa soft tissue stiffness, which was suitable as a scaffold for cell proliferation, migration, and differentiation.[13]

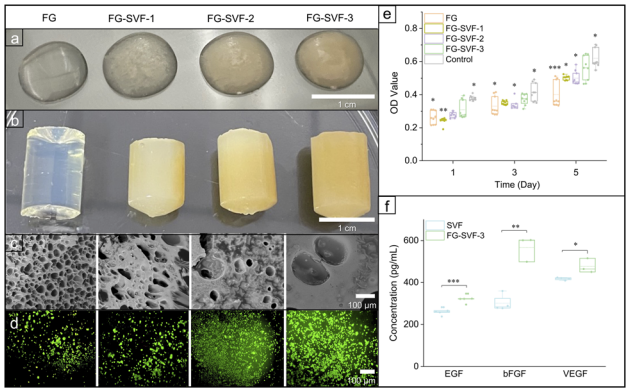

Fig. 2 (a and b) Photographs of the FG, FG-SVF-1, FG-SVF-2, and FG-SVF-3 hydrogels (a) before and (b) after photo-crosslinking. (c) SEM images of the FG, FG-SVF-1, FG-SVF-2, and FG-SVF-3 hydrogels. (d) Representative live/dead cell staining micrographs of the fibroblasts on FG, FG-SVF-1, FG-SVF-2, and FG-SVF-3 hydrogels. The live and dead cells were stained with AM (green) and PI (red), respectively. (e) The proliferation of fibroblasts on the FG, FG-SVF-1, FG-SVF-2, and FG-SVF-3 hydrogels after culture for 1, 3, and 5 days. $*P < 0.05$, $**P < 0.01$, and $***P < 0.001$ indicate the significant differences when compared with FG-SVF-3. (f) EGF, bFGF, and VEGF secretion from SVF and FG-SVF-3 hydrogels. $*P < 0.05$, $**P < 0.01$, and $***P < 0.001$ indicate the significant differences between SVF and FG-SVF-3.

Cell proliferation was examined after days 1, 3, and 5 of incubation. As expected, green fluorescence (live cells) was shown in the significant area of the images, while red fluorescence (dead cells) was rare, indicating hydrogels possessed superior biocompatibility and had a minor toxicity effect on cells (Fig. 2d and e).

In addition, the cells proliferated in each hydrogel group from day 1 to day 5, and the OD values of FG-SVF-3 were higher than those of the other hydrogels at each time point, which may be attributed to the regenerative properties of SVF and larger pore size of the hydrogel exerting a synergetic effect on cell proliferation. The pore size of cell growth is required in a wide range of 5–500 μm,[14] generally, a larger pore size could enhance the cell proliferation and migration.[15,16] According to cell proliferation and viability results, the FG-SVF-3 hydrogel was more suitable for cell growth than FG, FG-SVF-1, and FG-SVF-2 groups, and therefore the FG-SVF-3 hydrogel was selected for subsequent studies.

To explore the degradability of FG-SVF-3, *in vitro* degradation studies were conducted to mimic physiological conditions. The weight of FG-SVF-3 and FG decreased dramatically with increasing incubation time (Fig. S2 and S3†). The degradation rate of FG-SVF-3 reached 50% approximately for 8 days, which created space for the regeneration of new tissues, while the remaining hydrogel was able to continue promoting wound healing. The integrity of FG-SVF-3 decreased by 80% in 2 weeks, which was in agreement with the wound healing progress (around 2 weeks), suggesting that the hydrogel was a perfect match for the process of tissue regeneration. The degradation rate of the FG was slightly lower than that of FG-SVF-3, which could be explained by the addition of SVF, which affected the

formation of new bonds between the $-NH_2$ group in gelatin and the methacrylate group by photo-crosslinking, resulting in a slightly faster degradation rate of FG-SVF-3.

The three-dimensional porous structure of the hydrogel can mimic the native extracellular matrix (ECM), providing an ideal environment for SVF to promote wound healing through paracrine growth factors. To reveal the paracrine products of SVF in hydrogels, we detected the epidermal growth factor (EGF), fibroblast growth factor (bFGF), and vascular endothelial growth factor (VEGF) associated with tissue repair by enzyme-linked immunosorbent assay (ELISA). The results showed the secretion level of the growth factors was higher in FG-SVF-3 than that in SVF without the hydrogel, which indicated that the prepared hydrogel could promote the paracrine function of SVF (Fig. 2f). The healing-promoting ability of the composite hydrogels was detected using the Sprague-Dawley (SD) rat (n = 3) skin wound model.[17] Four circular complete skin defects 1.5 cm in diameter were prepared on both sides of the dorsal spine for each rat to minimize the interference of individual differences in wound healing.

The wound administered with gauze, FG, FG-SVF-3, or without treatment as control was recorded on days 0, 3, 7, 10, and 15 (Fig. 3a and b) and converted into numerical values (Fig. 3c). The results demonstrated that the FG-SVF-3 possessed more extraordinary wound healing ability than other groups within 15 days. Specifically, on day 3, the wound healing rate of FG-SVF-3 (58.13%) was significantly higher than those of the control (52.50%), gauze (47.09%), and FG (54.82%) groups. On days 7, 10, and 15, the wound healing ability of FG-SVF-3 was more pronounced than in other groups. In particular, on day 15, the trauma closure rate of FG-SVF-3 reached 96.78%.

To further explore the wound healing mechanism of FG-SVF-3, the expression of EGF, bFGF, and VEGF in the wound tissues was assessed on day 3 and day 7 (Fig. 3d and e). EGF is a peptide consisting of 53 amino acid residues that promote epithelial cell proliferation and ECM synthesis, which is the basis of accelerated wound healing.[11] At day 3, the EGF expression in FG-SVF-3 (185.76 ± 2.63 pg mL^{-1}) was higher than those in control, gauze, and FG groups, which were 176.05 ± 3.55 pg mL^{-1}, 161.88 ± 7.04 pg mL^{-1}, and 177.36 ± 3.99 pg mL^{-1}, respectively. At day 7, the EGF expression in FG-SVF-3 (191.27 ± 10.06 pg mL^{-1}) was still higher than in other groups. As an essential vascular growth factor, bFGF plays a significant role in wound healing, including stimulating fibroblast growth and proliferation, regulating collagen metabolism, stimulating endothelial cell division, and triggering vascular regeneration.[18] VEGF is a mitogenic stimulating factor and chemokine for endothelial cells, stimulating endothelial cell growth and displaying synergistic effects with bFGF to promote wound vascularization for wound repair.[19] On day 3, the expressions of bFGF and VEGF in FG-SVF-3 were significantly higher than in control, gauze, and FG groups. On day 7, the expression of bFGF and VEGF in FG-SVF-3 presented a similar profile to the results on day 3. The above results indicated that the FG-SVF-3 hydrogel can promote the regeneration of epithelial and vascular tissue, thus accelerating wound healing.

Regeneration and repair of skin tissues include epithelialization, where the differentiation and migration of epithelial cells at the wound site continues to form a new epidermal layer to cover the wound, and dermal remodeling, where the fibroblast cells proliferate at the trauma site, and collagen is deposited to reshape the dermis.[20,21] These processes can be observed by hematoxylin–eosin (H&E) and Masson's trichrome staining (Fig. 4a and b). H&E staining was performed on day 15 to characterize the remodelling of epidermal and subcutaneous tissue. Fig. 4a shows that the control and gauze groups formed an incomplete epidermal layer, whereas FG and FG-SVF-3 exhibited complete re-epithelialization followed by a process in the remodelling stage, leading to attachments such as hair follicles and vascular tissue. On day 15, the control and gauze groups exhibited disorganized collagen and poor epithelial cell formation, while the FG and FG-SVF-3 groups displayed uniform skin thickness. The skin thicknesses of the control, gauze, and FG groups were 43.9 ± 1.2 μm, 47.6 ± 2.4 μm, and 55.1 ± 0.2 μm, respectively, which were thinner than the FG-SVF-3 group (65.9 ± 4.3 μm) (Fig. 4d), which was in agreement with the profile of wound healing rate. Masson's trichrome staining makes collagen dark blue, which was employed to evaluate the amount of collagen deposition in wounds. In Fig. 4b, the wound tissue applied with FG-SVF-3 indicated that the regenerated collagen fibers on the wound were arranged, whereas other treatments showed sparse and disordered collagen production. On day 15, Col-1 and CD31 immunofluorescence staining was used to determine collagen and angiogenesis during wound healing.[22] The high CD31 and

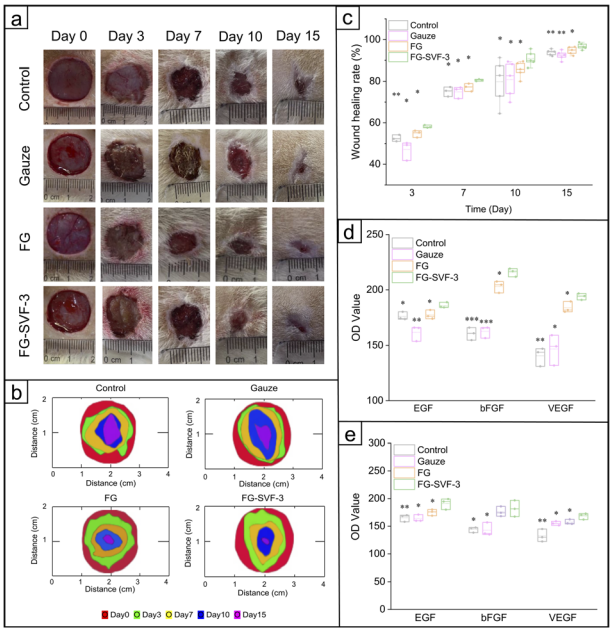

Fig. 3 (a) Representative photographs of the wound healing process at different times. (b) Schematic of wound healing with different treatments for 15 days. (c) Wound healing rates with different treatments after 3, 7, 10, and 15 days. (d and e) EGF, bFGF, and VEGF secretion in wounds was applied with control, gauze, FG, and FG-SVF-3 dressings on (d) day 3 and (e) day 7. *P < 0.05, **P < 0.01, and ***P < 0.001 indicate the significant differences when compared with FG-SVF-3.

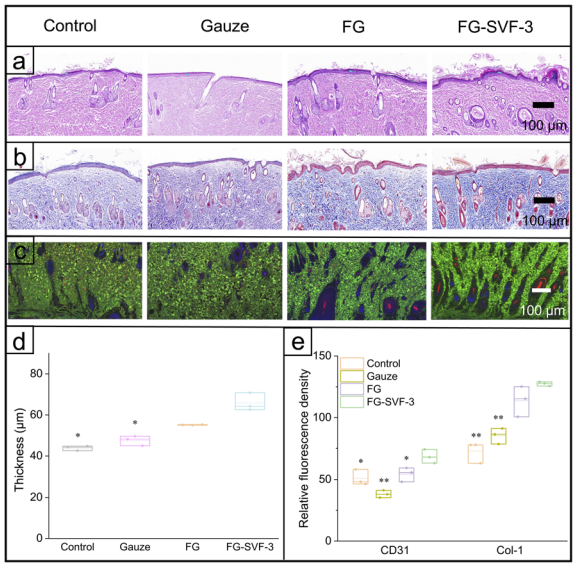

Fig. 4 (a) H&E staining, (b) Masson's trichrome staining, and (c) CD31 and Col-1 staining micrographs of the wounds treated with control, gauze, FG, and FG-SVF-3 groups on day 15. Red and green represent the blood vessels and collagen, respectively. (d) The epidermal thickness, (e) relative fluorescence density of CD31 and collagen expression for different wounds on day 15. *P < 0.05, and **P < 0.01 indicate the significant differences when compared with FG-SVF-3.

Col-1 expression levels were observed in the FG-SVF-3 group (Fig. 4e), indicating the formation of mature collagen and capillaries. This could be related to the paracrine effect of SVF, which promoted the regeneration of collagen fibers and vascular tissues for wound repair. These results demonstrated the SVF composite gelatin hydrogel can accelerate wound healing, increase the thickness of the regenerated epidermis, and promote the formation of type I collagen and dermal blood vessels.

Experimental section

Materials

Tilapia fish skins were purchased from Nanjing Sincere Frozen Food Company. Acetic acid was acquired from Macklin (Shanghai, China). Trypsin was supplied by Solarbio (Beijing, China). Dulbecco's Modified Eagle's Medium (DMEM) and Dulbecco's Modified Eagle's Medium/Nutrient Mixture F-12 (DMEM/F-12) were purchased from Sigma-Aldrich (USA). Fetal bovine serum (FBS) was bought from Gibco (USA). All the other chemicals used were analytical grade and obtained from Beijing Chemical Reagent Co., Ltd. (Beijing, China).

Methods

Synthesis of fish skin gelatin (FG). Tilapia skin (2 × 2 cm^2) was used as a raw material after removing the inner fascia, fat, and excess fish flesh. The skin was repeatedly rinsed with physiological saline and ultrapure water until the rinsing solution was clear. Then, the fish skin was placed in a −80 °C refrigerator and 37 °C water bath repeatedly 3 times, and sequentially placed in hypertonic saline (10% aqueous sodium chloride solution) and isotonic solution (ultrapure water) for 24 h to accelerate the fragmentation of cell structure. Next, the fish skin was placed in the trypsin solution, stirred for 30 min (1000 rpm), and washed with ultrapure water to obtain the decellularized fish skin gelatin matrix. The decellularized fish gelatin matrix was stirred for 4 h at 55 °C and lyophilized to obtain the fish skin gelatin.

Preparation of the hydrogel precursor solution and fish skin gelatin-derived hydrogels

Briefly, 3 g fish skin gelatin was added in 60 °C PBS and stirred for 1 h until the gelatin was completely dissolved into a clear yellow liquid to obtain the solution of fish skin gelatin. MA gelatin solution was prepared by dropping 94% methacrylic acid aqueous solution into the obtained liquid using a pump in the dark, and the fish skin-derived methacrylate-anhydride gelatin (GelMA) was obtained by freeze-drying. The GelMA was dissolved in a 0.25% (w/v) acyl phosphate photo-initiator to obtain a 40% hydrogel precursor solution and exposed to UV for 2 min to form a 0.2 cm thick fish skin gelatin-derived hydrogel.

The collection and extraction of SVF

SVF was collected and extracted following the previously reported protocol.[11] Briefly, a 3 mm porous cannula was used for extracting adipose tissues and centrifuged at 2700 rpm for 3 min, followed by removing the blood portion at the bottom. Then, the denser liquid portion (blood containing red blood cells) was discarded, and the ECM/SVF and supernatant oil portions were kept. The reserved materials were mixed and manually emulsified at 10 mL s^{-1} for 1 min using two 20 mL syringes connected by a 2.4 mm inner diameter connector to obtain celiac fat. The celiac fat was centrifuged at 3450 rpm for 3 min, and the gel-like material below the oil layer was SVF.

Synthesis and structural observation of the composite SVF hydrogels

The extracted SVF was added to the hydrogel precursor solution with different proportions (10%, 20%, and 30% (w/v), respectively) under aseptic conditions and shaken thoroughly to obtain photo-crosslinked pre-soluble gels. Then, the composite hydrogels with different ratios of SVF (FG-SVF-1, FG-SVF-2, and FG-SVF-3) were obtained after UV irradiation for 2 min. The FG, FG-SVF-1, FG-SVF-2, and FG-SVF-3 hydrogels were freeze-dried and cut into 2 × 2 × 2 mm^3 cubes. A scanning electron microscope (SEM, Hitachi, Japan) was used to observe the structures of different samples at an accelerating voltage of 15 kV.

Compression mechanical measurement

The compression properties of FG, FG-SVF-1, FG-SVF-2, and FG-SVF-3 hydrogels were evaluated by a compression fracture test. The hydrogels were made into cylindrical shapes (20 × 100 mm^2). The compressive strength was evaluated using a general-purpose testing machine (SENS, 6104), and the samples were compressed at a speed of 30 mm min^{-1} until they fractured. The

fracture strain values were calculated. Measurements were repeated 3 times for each sample, and all values were reported as mean ± standard deviation.

In vitro cytotoxicity assay

0.2 g of FG, FG-SVF-1, FG-SVF-2, and FG-SVF-3 hydrogels were placed in a 24-well plate, sterilized by UV irradiation, and washed 3 times with PBS. Then DMEM medium containing 10% FBS and 1% penicillin/streptomycin was added to each well. The L929 fibroblasts were seeded in each well at 1×10^4 cells and incubated at 37 °C. Cell proliferation was detected on days 1, 3, and 5 using the CCK-8 kit and enzyme marker.

L929 fibroblasts cultured for 3 days were stained using the Live/dead cell staining kit. The cells were observed under a fluorescence microscope (IX53, Olympus, Japan). Live cells were labelled with green fluorescence, and dead cells were labelled with red fluorescence. Measurements were repeated 3 times, and all values are reported as mean ± standard deviation.

Determination of the secretion of EGF, bFGF, and VEGF

SVF and FG-SVF-3 hydrogel containing the same amount of SVF were placed into 25 cm^2 T25 culture bottles with the addition of DMEM/F-12 complete medium and incubated for 24 h. Then, the culture medium was changed to DMEM/F-12 without FBS for another 24 h treatment. Each solution was centrifuged at 1600 rpm for 10 min, and the supernatant was collected. The EGF, bFGF, and VEGF content in the supernatant solution was measured by the ELISA kit. Measurements were repeated 3 times, and all values were reported as mean ± standard deviation.

Degradation of the hydrogels

Lyophilized hydrogels with the same initial mass (W_0) were exposed to PBS solution in a 37 °C shaker. On days 1, 2, 4, 8, 12, 21, and 28, the remaining mass (W_t) of samples was recorded to calculate the degradation rates. The degradation rate (%) of the hydrogels was calculated using the following equation:

$$\text{Degradation rate } (\%) = \frac{W_0 - W_t}{W_0} \times 100\% \quad (1)$$

Meanwhile, the hydrogels were retained at each time point. SEM was used to observe the structures of the samples under an accelerating voltage of 15 kV.

In vivo investigation

The healing-promoting ability of the composite hydrogels was assessed using the SD rat ($n = 3$) skin wound model. Forty male SD rats (weighing 280–300 g) were prepared, anesthetized intraperitoneally with 10% chloral hydrate, and then depilated. Four round full-thickness skin defects (1.5×1.5 cm^2) were formed on both sides of the dorsal spine of each rat to minimize the individual differences of the rat. FG-SVF-3 hydrogel was applied to the defects to evaluate its ability to promote wound healing, and FG, gauze, and blank groups were used as controls. Images of wounds were taken on days 0, 3, 7, 10, and 15, and the wound healing rate was analyzed using ImageJ software (Version 1.53). Four rats were randomly executed on days 3, 7, 10, and 15, and wound tissue was excised along the edges. Half of the dissected tissue was paraffin-embedded for histological staining, and the rest was rapidly frozen and stored at −80 °C for quantitative analysis of tissue growth factors. Measurements were repeated 3 times, and all values were reported as mean ± standard deviation.

H&E staining was performed on tissue samples to observe morphological changes. Masson's trichrome staining was used to assess the defect repair and collagen formation. Immunofluorescence staining was performed using anti-CD31 and anti-Col-1 antibodies to assess neovascularization and collagen synthesis. ImageJ software was used to calculate the numerical value of CD31-positive neovascularization and Col-1-positive collagen fibers. Measurements were repeated 3 times, and all values were reported as mean ± standard deviation.

The frozen tissues on days 3 and 7 were washed with cold PBS (0.01 M, pH = 7.4) to remove residual blood, and then equal weights of the tissue were chopped. The chopped tissues were mixed with PBS containing a protease inhibitor at a ratio of 1 : 9 (w/v), subsequently added to a glass homogenizer, and ground thoroughly. The homogenate was centrifuged at 5000*g* for 5–10 min, and the supernatant was used for the determination of the EGF, bFGF, and VEGF using ELISA kits, respectively. Measurements were repeated 4 times, and all values were reported as mean ± standard deviation.

Human adipose tissue was obtained from patients who underwent abdominal liposuction at The Affiliated Hospital of Qingdao University. All protocols were approved by the Ethics Committee of The Affiliated Hospital of Qingdao University. All animal experiments were approved by the Animal Ethics Committee of Qingdao University and were performed according to the guidelines of the National Health and Medical Research Council (China).

Statistical analyses

One-way analysis of variance was used to compare the groups, and all subsequent pairwise comparisons were performed using the Student's *t*-test.

Conclusions

In conclusion, we prepared SVF-rich tilapia skin hydrogels with excellent mechanical properties and degradation rates consistent with wound healing. Meanwhile, we found that the FG-SVF-3 hydrogel could promote the paracrine function of SVF and provide a favorable microenvironment for cell growth. *In vivo* studies have shown that the FG-SVF-3 hydrogel can effectively promote the expression of EGF, bFGF, and VEGF and accelerate the regeneration of epithelial tissues, blood vessels, and type I collagen, thus accelerating rapid wound healing. In summary, the FG-SVF-3 hydrogel generated in this study has a strong capacity to promote the healing of full-thickness wounds and is expected to be a biological dressing for wound therapy.

Data availability

The data that support the findings of this study are available from the corresponding author upon reasonable request.

Author contributions

Yanan Luo: conceptualization, methodology, data curation, writing – original draft. Manfei Fu: methodology, data curation, writing – original draft. Ziyi Zhou, Xiaopei Zhang: investigation, methodology, data curation. Qingxia Guo, Yawen Wang, Weina Zhang: methodology, data curation. Yuanfei Wang: supervision, writing – review & editing, funding acquisition. Zhenyu Chen: supervision, project administration. Tong Wu: conceptualization, resources, supervision, project administration, writing – review & editing, funding acquisition.

Conflicts of interest

There are no conflicts to declare.

Acknowledgements

This work was supported by the Natural Science Foundation of Shandong Province (ZR2021YQ17), Special Funds for Taishan Scholars Project of Shandong Province (No. tsqn202211125), Qingdao Key Health Discipline Development Fund (2022–2024), Qingdao Clinical Research Center for Oral Diseases (22-3-7-lczx-7-nsh), and Shandong Provincial Key Medical and Health Discipline of Oral Medicine (2024–2026). The authors also thank the "Advanced Biomaterials and Regenerative Medicine (ABRM)" Innovation Team supported by the Young-Talent Introduction and Cultivation Plan in the Universities of Shandong Province.

References

1 J.-Y. Ding, M.-J. Chen, L.-F. Wu, G.-F. Shu, S.-J. Fang, Z.-Y. Li, X.-R. Chu, X.-K. Li, Z.-G. Wang and J.-S. Ji, Mesenchymal stem cell-derived extracellular vesicles in skin wound healing: roles, opportunities and challenges, *Mil. Med. Res.*, 2023, **10**(1), 36.

2 P. Bourin, B. A. Bunnell, L. Casteilla, M. Dominici, A. J. Katz, K. L. March, H. Redl, J. P. Rubin, K. Yoshimura and J. M. Gimble, Stromal cells from the adipose tissue-derived stromal vascular fraction and culture expanded adipose tissue-derived stromal/stem cells: a joint statement of the International Federation for Adipose Therapeutics and Science (IFATS) and the International Society for Cellular Therapy (ISCT), *Cytotherapy*, 2013, **15**(6), 641–648.

3 C. Spilleboudt, V. De Wilde, P. Lewalle, L. Cabanne, M. Leclerc, F. Beckerich, D. Bories, S. Cardoso, M. P. Soares and B. Vokaer, Donor-derived myeloid heme oxygenase-1 controls the development of graft-versus-host disease, *Front. Immunol.*, 2021, **11**, 579151.

4 I.-S. Park, P.-S. Chung and J. C. Ahn, Enhanced angiogenic effect of adipose-derived stromal cell spheroid with low-level light therapy in hind limb ischemia mice, *Biomaterials*, 2014, **35**(34), 9280–9289.

5 G. Jin, W. Li, F. Song, J. Zhao, M. Wang, Q. Liu, A. Li, G. Huang and F. Xu, Fluorescent conjugated polymer nanovector for *in vivo* tracking and regulating the fate of stem cells for restoring infarcted myocardium, *Acta Biomater.*, 2020, **109**, 195–207, DOI: **10.1016/j.actbio.2020.04.010**.

6 J. Cai, H. Zhang, Y. Hu, Z. Huang, Y. Wang, Y. Xia, X. Chen, J. Guo, H. Cheng and L. Xia, GelMA-MXene hydrogel nerve conduits with microgrooves for spinal cord injury repair, *Journal of Nanobiotechnology*, 2022, **20**(1), 460; Y. Chen, X. Wang, S. Tao, Q. Wang, P.-Q. Ma, Z.-B. Li, Y.-L. Wu and D.-W. Li, Research advances in smart responsive-hydrogel dressings with potential clinical diabetic wound healing properties, *Mil. Med. Res.*, 2023, **10**(1), 37.

7 D. Liu, M. Nikoo, G. Boran, P. Zhou and J. M. Regenstein, Collagen and gelatin, *Annu. Rev. Food Sci. Technol.*, 2015, **6**, 527–557; Y. Liu, Q. Guo, X. Zhang, Y. Wang, X. Mo and T. Wu, Progress in electrospun fibers for manipulating cell behaviors, *Adv. Fiber Mater.*, 2023, **5**(4), 1241–1272.

8 R. J. Shakila, E. Jeevithan, A. Varatharajakumar, G. Jeyasekaran and D. Sukumar, Comparison of the properties of multi-composite fish gelatin films with that of mammalian gelatin films, *Food Chem.*, 2012, **135**(4), 2260–2267.

9 Y. Luo, F. Tao, J. Wang, Y. Chai, C. Ren, Y. Wang, T. Wu and Z. Chen, Development and evaluation of tilapia skin-derived gelatin, collagen, and acellular dermal matrix for potential use as hemostatic sponges, *Int. J. Biol. Macromol.*, 2023, **253**, 127014.

10 L. Shang, F. Fu, Y. Cheng, Y. Yu, J. Wang, Z. Gu and Y. Zhao, Bioinspired multifunctional spindle-knotted microfibers from microfluidics, *Small*, 2017, **13**(4), 1600286.

11 M. Sun, Y. He, T. Zhou, P. Zhang, J. Gao and F. Lu, Adipose extracellular matrix/stromal vascular fraction gel secretes angiogenic factors and enhances skin wound healing in a murine model, *BioMed Res. Int.*, 2017, **2017**, 3105780.

12 E. Nicol, Photopolymerized Porous Hydrogels, *Biomacromolecules*, 2021, **22**(4), 1325–1345, DOI: **10.1021/acs.biomac.0c01671**; R. Foudazi, R. Zowada, I. Manas-Zloczower and D. L. Feke, Porous hydrogels: present challenges and future opportunities, *Langmuir*, 2023, **39**(6), 2092–2111.

13 C. Li, G. Guan, R. Reif, Z. Huang and R. K. Wang, Determining elastic properties of skin by measuring surface waves from an impulse mechanical stimulus using phase-sensitive optical coherence tomography, *J. R. Soc., Interface*, 2012, **9**(70), 831–841.

14 S. Yang, K.-F. Leong, Z. Du and C.-K. Chua, The design of scaffolds for use in tissue engineering. Part I. Traditional factors, *Tissue Eng.*, 2001, **7**(6), 679–689.

15 F. Gnanaprakasam Thankam and J. Muthu, Alginate based hybrid copolymer hydrogels—Influence of pore morphology on cell–material interaction, *Carbohydr. Polym.*, 2014, **112**, 235–244.

16 S. H. Oh, T. H. Kim, G. I. Im and J. H. Lee, Investigation of pore size effect on chondrogenic differentiation of adipose stem cells using a pore size gradient scaffold, *Biomacromolecules*, 2010, **11**(8), 1948–1955.

17 C. He, X. Liu, Z. Zhou, N. Liu, X. Ning, Y. Miao, Y. Long, T. Wu and X. Leng, Harnessing biocompatible nanofibers and silver nanoparticles for wound healing: Sandwich wound dressing *versus* commercial silver sulfadiazine dressing, *Mater. Sci. Eng., C*, 2021, **128**, 112342.

18 M. J. van Velthoven, A. N. Gudde, F. Struijs, E. Oosterwijk, J.-P. Roovers, Z. Guler, C. R. Hooijmans and P. H. Kouwer, The effect of growth factors on vaginal wound healing: a systematic review and meta-analysis, *Tissue Eng., Part B*, 2023, **29**(4), 429–440.

19 K. E. Johnson and T. A. Wilgus, Vascular endothelial growth factor and angiogenesis in the regulation of cutaneous wound repair, *Adv. Wound Care*, 2014, **3**(10), 647–661.

20 X. Liu, Q. Wei, Z. Sun, S. Cui, X. Wan, Z. Chu, Y. Zhang, W. Zhong, L. Lu and L. Shi, Small extracellular vesicles: Yields, functionalization and applications in diabetic wound management, *Interdisciplinary Medicine*, 2023, **1**(4), e20230019.

21 H. Kim, W. H. Kong, K.-Y. Seong, D. K. Sung, H. Jeong, J. K. Kim, S. Y. Yang and S. K. Hahn, Hyaluronate Epidermal Growth Factor Conjugate for Skin Wound Healing and Regeneration, *Biomacromolecules*, 2016, **17**(11), 3694–3705.

22 N. Liu, Z. Zhou, X. Ning, X. Zhang, Q. Guo, M. Guo, Y. Wang and T. Wu, Enhancing the paracrine effects of adipose stem cells using nanofiber-based meshes prepared by light-welding for accelerating wound healing, *Mater. Des.*, 2023, **225**, 111582.